energies

MDPI

Article

Research on the Coordinated Recovery Strategy Based on Centralized Electric Vehicle Charging Station

Menghao Wen [1], Huabo Shi [2,3], Baohong Li [1,*], Qin Jiang [1], Tianqi Liu [1] and Chaofan Ding [1]

[1] College of Electrical Engineering and Information Technology, Sichuan University, Chengdu 610065, China; 2020141440339@stu.scu.edu.cn (M.W.); jiangqin_jq@126.com (Q.J.); 2020141440189@scu.edu.cn (C.D.)
[2] Power Internet of Things Key Laboratory of Sichuan Province, Chengdu 610072, China; shbo87@163.com
[3] State Grid Sichuan Electric Power Research Institute, Chengdu 610041, China
* Correspondence: scu_lbh@163.com

Abstract: Electric vehicles have become a crucial component of modern power systems, possessing substantial energy reserves that can be important power supplies in blackouts where the power grid has weak reserves or limited connections to other grids. In order to clarify the technical conditions and control methods of the centralized electric vehicle charging station as the black-start power source of the power grid, assuming that the centralized electric vehicle charging station can be considered a single, large-scale energy storage system, this paper proposes a three-stage coordinated recovery strategy based on the centralized electric vehicle charging station. The strategy involves three distinct stages, beginning with the establishment of AC frequency and voltage by the electric vehicle charging station to initiate the auxiliary load of the power plant. In the middle stage, considering the traditional generator has been connected, the charging station's control mode is set to provide constant active and reactive power output, providing extra voltage and frequency support to the grid-connected generating units and crucial loads. Finally, in the later stage, control strategies are tailored to the charging power stations' capacities, with one group of additional oscillation damping controllers, while the other group adopts additional frequency control to decrease power disturbances, ensuring a smooth recovery of the power grid. A PSCAD/EMTDC-based model was constructed to verify the proposed coordinated grid recovery strategies. The results demonstrated that the centralized station successfully established the voltage and frequency of the AC system, and the designed additional controller also made the recovery process much more stable.

Keywords: electric vehicle charging station; black start; coordinated control; additional frequency control

Citation: Wen, M.; Shi, H.; Li, B.; Jiang, Q.; Liu, T.; Ding, C. Research on the Coordinated Recovery Strategy Based on Centralized Electric Vehicle Charging Station. *Energies* **2023**, *16*, 5401. https://doi.org/10.3390/en16145401

Academic Editor: Ahmed Darwish

Received: 11 June 2023
Revised: 3 July 2023
Accepted: 10 July 2023
Published: 15 July 2023

1. Introduction

Currently, the black start power supply is categorized into two main types: hydropower plants and fuel oil or gas power plants. In regions of southern China with abundant water resources, hydropower units are generally preferred as the primary choice for black-start power supply. However, water resources are limited in most parts of northern China, particularly in the northwest region. Hence, using hydropower stations as black-start power sources is not an optimal solution [1]. Furthermore, hydropower stations are typically located in remote areas far from the urban power grid, and the sluggish reaction rate of the hydropower unit speed control system restricts its regulation performance, thereby limiting its capacity as a black-start power supply to some extent. Additionally, fuel power plants or gas power plants typically have a lengthy start-up time, which leads to a prolonged recovery time for the entire network and a significant reduction in reliability as a black-start power supply. Once the entire power grid enters the all-black state, it would lead to the inability to power loads, causing a stagnation of nearly all industries in society, a loss of normalcy in people's lives, and incalculable political, economic, and societal losses. Consequently, the most crucial factors for assessing the efficacy of a black-start

power supply are its reliability and availability. Currently, with the expansion of electric vehicle applications, China has seen a significant increase in the number of centralized electric vehicle charging stations. Furthermore, as these charging stations are predominantly situated in urban areas close to load centers, they are capable of a faster load recovery during the power grid black-start process compared with hydropower, thermal power stations, etc. Furthermore, considering the rapid development of China's power electronics technology, battery technology, and other fields, electric vehicles are emerging as a key type of distributed power supply. The centralized electric vehicle charging station, therefore, has become an essential development direction in the new energy field as a power grid black-start power supply [2].

At present, the investigation into the decentralized energy supply of electric vehicles (EVs) centers predominantly on engaging in peak regulation and frequency modulation of the power grid, as well as demand response [3]. A vehicle-grid cooperative control strategy to engage in frequency modulation of the power grid was introduced in reference [4]. Ref. [5] proposed a coordinated operation method for a system containing electric vehicle charging stations and a distribution power network, considering integrated energy and reserve regulation, which can reduce the dispatching cost compared with the situation of purchasing energy and reserve directly from the wholesale market. Thus, we can conclude that the economic cost of a centralized electric vehicle charging station as a black start power source is lower than that of purchasing energy and reserves in the market. Literature [6] compared and analyzed four different charging management strategies for electric vehicles and confirmed that the management of the charging process for electric vehicles can reduce the overall cost of the charging process by more than 30%. Ref. [7] examined the number of batteries required to be reserved for the centralized electric vehicle charging station to utilize battery capacity. In conclusion, when the battery capacity accessible in the centralized electric vehicle charging station attains a specific level, it can supply unit start-up power for the regional power system, which has no black-start power supply or insufficient black-start capacity, to assist in system recovery. And it can reduce the cost of a black startup.

During the black start, the system characteristics and control methods differ significantly from normal operation. At present, research on black start both domestically and abroad primarily focuses on the integration of new energy systems such as wind power and photovoltaic to assist the grid in completing black start [8–10]. In Ref. [11], a scheme and real-time scheduling strategy for multi-type distributed resources in distribution networks were proposed to assist in the black start of key nodes in the primary network. This strategy ensures the safe and stable recovery of power supply in the shortest amount of time, thereby confirming the availability of distributed power supply during the black start of the power grid. Literature [12] discussed the black start step, system structure, and control strategy of wind-storage combined systems and established a structure for a wind-storage combined system with DC voltage. This confirms the vital role of energy storage systems in the black start of the power grid.

However, there is a dearth of studies on the potential for electric vehicle charging stations to serve as a black start power supply to assist in power system restoration both domestically and internationally. In Ref. [13], a grid reconfiguration model based on bi-level optimization was constructed to determine the recovery time and recovery path of the generator set with the electric vehicle charging station as the black-start power source to aid in grid recovery. Nevertheless, any auxiliary functions of the charging station after the generator set's recovery during the black start process remain unexplored.

From the above research, it can be seen that the present studies usually concentrate on traditional recovery methods. Although some black start discussions have been concerned with renewable energies, few black start analyses have been done around electric vehicle charging stations. The capacity of centralized electric vehicle charging stations has reached tens of megawatts, which can cover the auxiliary equipment's capacity of the power plant. So that the black start based on the centralized electric vehicle charging stations can be

conducted. Under the above background, to provide a more reliable and accessible black-start power supply for the black-start of the power grid and offer some new ideas for the coordinated control strategy of electric vehicles and the power grid in the future, this paper presents a three-stage coordinated recovery strategy for the black start of power grid based on a centralized electric vehicle charging station under blackout.

The novelties of the proposed strategy can be summarized as follows.

(1) The black-start strategy based on the electric vehicle charging stations is varied in different stages, where the aims of each stage are different and the functions of the controllers are also varied.
(2) The state of charge (SOC) of different electric vehicle charging stations is considered in the recovery process to make sure stations with different SOCs can play varied roles in the black start control.
(3) The multiple additional controllers are designed for different electric vehicle charging stations, which can not only suppress the oscillations caused by weak damping but also decrease the frequency fluctuatations caused by power shortages.

The proposed strategy is verified through simulation of a combined system model of electric vehicle charging and storage power stations built on the PSCAD/EMTDC platform. The simulation results verify the efficiency and correctness of the proposed strategy.

The rest of this paper is organized as follows. Section 2 presents the basic structure of the centralized electric vehicle charging station. In Section 3, the coordinated recovery strategy is explained in detail. Furthermore, Section 4 builds a combined system model of electric vehicle charging and storage power stations on the PSCAD/EMTDC platform and verifies the efficiency and correctness of the proposed strategy. Finally, conclusions are drawn in Section 5.

2. Basic Structure of the Centralized Electric Vehicle Charging Station

When utilized as a black start power supply, the centralized charging station can serve as a large-capacity energy storage system that functions as the DC reserve power supply of the system. Through a direct connection to the grid bus via VSC, the station can swiftly respond to the requirements of the voltage amplitude and system frequency support during the grid's black start. The basic structure is shown in Figure 1.

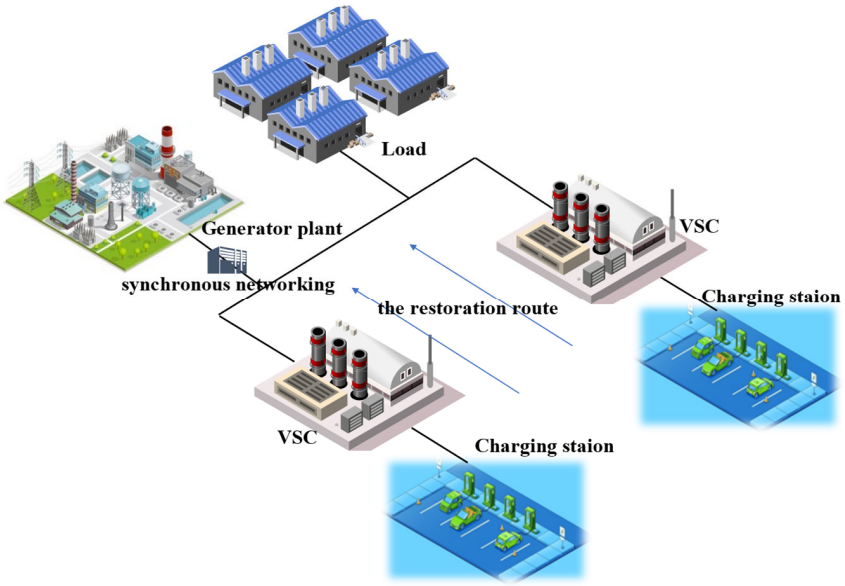

Figure 1. Centralized Electric Vehicle Charging and Station Joint System.

The centralized electric vehicle charging station is mainly composed of a battery system (BS) and a power conversion system (PCS). The charging station's BS is established

by several single cells in series [14], which can be modeled as the general circuit illustrated in Figure 2.

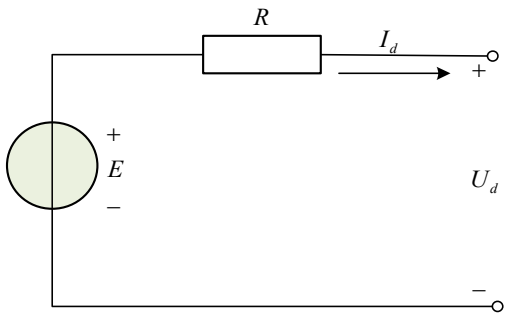

Figure 2. Genetic equivalent circuit of model battery.

Where U_d and I_d represent the port voltage and current of the battery, respectively. E is a controlled voltage source. R is usually given by the battery manufacturer, assuming it remains unchanged during operation. E can be expressed as:

$$E = E_0 - K\frac{C_{\max}}{C_{\max} - Q_e} + A\exp(-B \times Q_e) \tag{1}$$

where E_0 is internal potential (V); $C_{\max}$ is the maximum capacity of battery; Q_e is discharge quantity; $AV, B(\mathrm{Ah})^{-1}, K(\mathrm{V})$ are fitting parameters; $Aexp(-B \times Q_e)$ describes the exponential characteristics of the initial discharge stage of the battery; $K\frac{C_{\max}}{C_{\max}-Q_e}$ describes the rated characteristic region of battery discharge characteristics.

The PCS mainly constitutes a voltage source converter (VSC), which enables the bidirectional energy transfer between the centralized electric vehicle charging station and the AC grid. Its basic topological structure is shown in Figure 3, where U_{dc} represents the electric vehicle charging station port's output voltage, S1~S6 denotes the IGBT switch, and R, L, and C designate the filter's internal resistance, inductance, and capacitance, respectively.

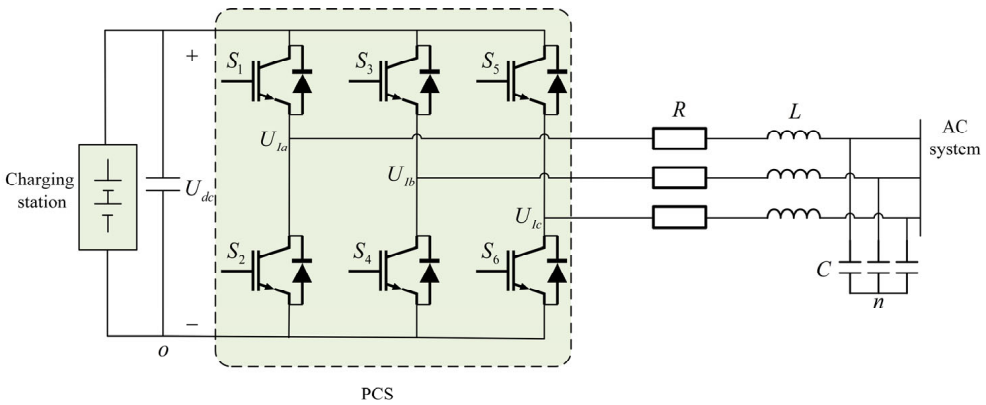

Figure 3. Basic structure of PCS.

Research findings indicate that only active power exchange occurs between the centralized electric vehicle charging station and the AC power grid [15,16]. The PCS primarily determines the reactive power, and the active and reactive power exchange between the PCS and the power grid can be mathematically expressed as follows:

$$\begin{cases} P_B = \frac{U_S U_I}{X}\sin\delta \\ Q_B = \frac{U_S(U_S - U_I\cos\delta)}{X_C} \end{cases} \tag{2}$$

In the formula, U_S is the bus voltage amplitude of the charging station, U_I is the voltage amplitude of the inverter AC side in PCS, X_C is the equivalent reactance between

the charging station and the bus of the grid-connected point, δ is the phase angle difference between the inverter AC side voltage and the bus voltage of the grid-connected point in PCS, P_B *and* Q_B are the active and reactive output of the charging station.

According to Equation (2), adjusting δ and U_I can quickly change the active and reactive power output of the charging station like the power grid, and its power limit can be expressed as:

$$\begin{cases} |P_B| \le P_{\max} \\ |Q_B| \le \sqrt{S_{VSC}^2 - P_B^2} \end{cases} \tag{3}$$

where P_{max} is the maximum charging and discharging power of the charging station; and S_{VSC} is the capacity of the inverter in PCS.

According to ref. [17], in order to prevent electric vehicle charging and storage power stations from experiencing overcharging or over-discharging, when the generator set is initiated, it is necessary to ensure that the state of charge (SOC) remains within a normal range. The maximum and minimum values of the state of charge of the charging station can be expressed as:

$$\begin{cases} SOC_{B\min} = SOC_0 - \frac{E_{0\max}}{E_B} \ge SOC_{\min} \\ SOC_{B\max} = SOC_0 - \frac{E_{0min}}{E_B} \le SOC_{\max} \end{cases} \tag{4}$$

In this formula, SOC_{max} and SOC_{min} respectively represent the upper and lower limits of the SOC of the charging station as the black-start power supply during normal operation; E_{0max} and E_{0min} represent the maximum and minimum cumulative energy output of the charging station relative to its initial state during the black-start process; and E_B is the rated capacity of the charging station.

Subtracting the two equations in Equation (4):

$$E_B \ge \frac{E_{0\max} - E_{0\min}}{SOC_{\max} - SOC_{\min}} \tag{5}$$

According to Equation (5), the rated capacity of the charging station can be expressed as the ratio of the difference between the maximum and minimum cumulative energy output to the set charge range. In theory, the greater the rated capacity of the charging station, the higher the reliability of the black start power supply of the power grid. However, considering economic factors, the minimum rated capacity of the charging station can be determined by this formula.

At the same time, the reactive power output from the electric vehicle charging station to the AC grid is mainly limited by the capacity of the PCS inverter and the active output of the charging station. Therefore, the capacity of the PCS inverter can be configured according to Equation (6):

$$S_{vsc} \ge \max\left(\sqrt{P_B^2 + Q_B^2}\right) \tag{6}$$

The specific configuration method can be found in Ref. [17].

3. Coordinated Recovery Strategy Based on Charging Station

3.1. Black Start Recovery Step

Black start refers to the process of using the unit's own internal self-starting ability to drive the power supply without self-starting ability, gradually restore the supply of the grid, and ultimately achieve the recovery of the entire power grid [18]. The black start process for the whole grid can be mainly divided into the following three steps:

(1) Black start power self-starting process.
(2) Line recovery stage. The charging stage of the line is mainly to use the black-start power supply (this article refers to the electric vehicle charging station) and internal equipment to stabilize the line voltage and frequency, and restore the auxiliary load of

the generator set in a short time, so that the generator set can be connected to the grid as soon as possible, laying the foundation for the subsequent comprehensive recovery.

(3) Receiving system recovery phase. The load recovery process is mainly to use the started generator set to quickly restore the important load and, in the recovery process, maintain the system frequency, node voltage, and so on within the limit value to ensure that the power grid will not have secondary power failure.

3.2. Control Method of the Electric Vehicle Charging Station in the Black Start Process

In this scheme, during the early stages of black start, the bus voltage and system frequency of the power grid are maintained by a V/f controlled charging station, and the charging station is used to charge the transmission line, line transformer, and generator set auxiliary load. After the generator set is connected to the grid, the charging station switches its control mode, and the voltage and frequency of the bus are maintained by the generator set, while the charging station acts as an auxiliary power source to maintain frequency stability during the subsequent power grid recovery process. The specific method is as follows:

(1) In the early stage of black start, the charging station system in Figure 4 adopts the V/f control strategy. By setting the voltage reference value U_{Bref} and frequency reference value f_{Bref} to 1, i.e., the bus voltage is fixed at 230 kV and the system frequency is 50 Hz, the charging station can stabilize the output voltage and frequency of electric vehicle charging and discharging stations at the rated value, thus providing stable voltage and frequency support for the isolated grid and maintaining the balance of active and reactive power [19].

(2) After the generator set is connected to the grid, the system frequency and voltage are supported by the generator set. Part of the electric vehicle charging stations with large residual capacity adopt the P/Q additional frequency control strategy shown in Figure 5 to suppress the large disturbance during the black start process. The mathematical expression is as follows:

$$P_B = P_{Bref} + K^* \Delta f \tag{7}$$

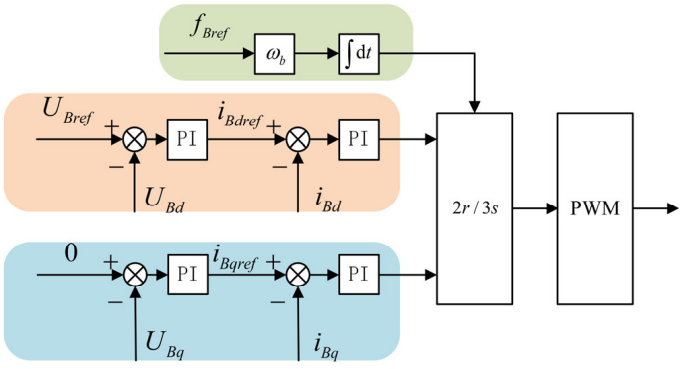

Figure 4. Control diagram of Charging station operating in island mode.

In the formula, P_{Bref} is the rated output active power of the charging station system, P_B is the actual output active power of the charging station system, Δf is the difference between the actual frequency of the AC system and the rated reference frequency, which is 50 Hz in this system, K^* is the frequency droop coefficient, which governs the influence degree of the system frequency fluctuation on the line power flow control quantity. Higher values of the coefficient lead to greater control over the output active power of the charging station, as well as an increased ability to absorb unbalanced power and suppress system frequency fluctuation. The control strategy relies on measuring frequency with a phase-locked loop, which adds a reference signal to the VSC's reference power and supports system frequency response through changes in output power [20]. The control strategy is

only applied to large frequency fluctuations, with a threshold of 0.5 Hz. If the frequency fluctuation exceeds this value, the charging station with a large remaining capacity provides power support to adjust the system frequency. Fluctuations below 0.5 Hz are adjusted by a P/Q additional lead-lag controller in a charging station with a small capacity.

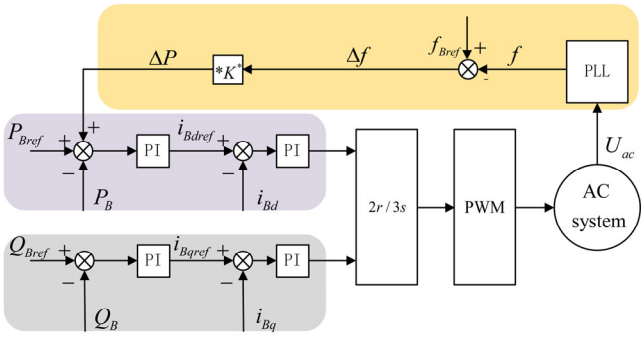

Figure 5. Additional frequency PQ control.

(3) The other part of the charging station with a small residual capacity adopts the P/Q additional lead-lag control shown in Figure 6 to deal with the low-frequency oscillation of the system caused by the multi-machine grid connection in the process of grid restoration. The lead-lag controller's specific structure is presented in Figure 7. After the band-pass filter, the actual value of the active power output of the charging station is affected by the system frequency fluctuation Δf through a lead-lag link, which is added to the reference value of the active power output of the charging station so as to adjust the frequency fluctuation caused by the small disturbance of the system.

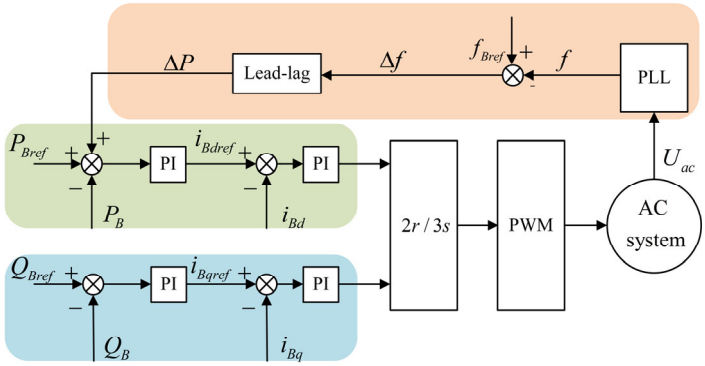

Figure 6. Additional lead-lag PQ control.

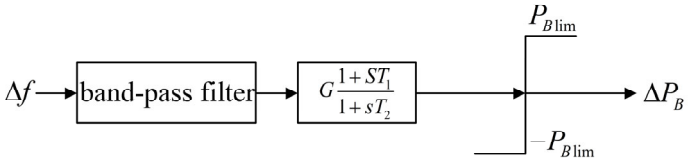

Figure 7. The specific structure of lead-lag controller.

To design the lead-lag controller, the system parameters must be identified first. This paper utilizes TLS-ESPRIT identification technology, which is a high-resolution signal analysis method known for its high computational efficiency and strong anti-interference ability. The ESPRIT algorithm collects the rotation factor, attenuation factor, and signal frequency of the signal calculated by the autocorrelation matrix and cross-correlation matrix formed by the identification data. The attenuation factor and signal frequency of the collected signal are obtained by identifying the rotation factor, and then the amplitude

and phase of the signal can be obtained by TLS [21]. Finally, the relevant parameters of the controller are obtained by using the linear inequality constraints to design the controller.

Assuming that the sampled signal K_a is obtained by sampling at time a, then the sampled signal can be represented by a row matrix $K = [k_0, k_1, L, k_{N-1}]$, and the following $L \times M$ Hankel matrix H is constructed:

$$\begin{bmatrix} k_0 & k_1 & k_2 & \cdots & k_{M-1} \\ k_1 & k_2 & \ddots & \cdots & \vdots \\ \vdots & \ddots & \ddots & \cdots & k_{N-2} \\ k_{L-1} & k_L & \cdots & k_{N-2} & k_{N-1} \end{bmatrix} \tag{8}$$

$N = L + M - 1$ is the length of the oscillation data. The singular value method is used to decompose the constructed H matrix:

$$H = U\Sigma V^H = \begin{bmatrix} U_S & U_N \end{bmatrix} \begin{bmatrix} \Sigma_S & 0 \\ 0 & \Sigma_N \end{bmatrix} \begin{bmatrix} V_S^H \\ V_N^H \end{bmatrix} \tag{9}$$

The subscripts S and N correspond to the signal space and the noise space, respectively. U is an $L \times L$ matrix, Σ is an $L \times M$ diagonal matrix, and the singular value of the Hankel matrix is the value of the diagonal element of Σ, which is arranged in descending order. Σ_S is a square matrix whose order is equal to the modal number P; V is the unitary matrix of $M \times M$, V^H is its conjugate transpose; according to the size of the singular value, the signal subspace V_S and the noise subspace V_N can be divided. The singular value of the signal space is much larger than that of the noise space, so if the signal does not contain noise or contains less noise, the size of the elements in the matrix V_N is almost zero. V_S is decomposed into two alternating subspaces V_1 and V_2.

$$V_S = \begin{bmatrix} V_1 \\ \cdots \end{bmatrix} = \begin{bmatrix} \cdots \\ V_2 \end{bmatrix} \tag{10}$$

The matrix $[V_1\ V_2]$ is established, and the matrix is decomposed by singular value to obtain V_P^H, which is divided into four square matrices of $P \times P$ dimension.

$$V_p^H = \begin{bmatrix} V_{11} & V_{12} \\ V_{21} & V_{22} \end{bmatrix} \tag{11}$$

The rotation matrix ψ_{TLS} can be calculated as $\psi_{TLS} = -V_{12}V_{22}^{-1}$. The eigenvalues of ψ_{TLS} are $\lambda = [\lambda_1, \lambda_2, L\lambda_P]$, where λ_i is the estimated value of the pole z_i. Furthermore, the characteristic parameters of each mode can be solved separately. The frequency f_i and the damping factor α_i are given by:

$$\begin{cases} f_i = \frac{\arctan(\mathrm{Im}(z_i)/\mathrm{Re}(z_i))}{2\pi\Delta t} \\ \alpha_i = -\frac{\ln|z_i|}{\Delta t} \end{cases} \tag{12}$$

where Δt is the sampling interval. These frequencies and attenuation factors correspond to the natural vibration modes of the system, and then they can be used to design an appropriate lead-lag controller.

The transfer function of the lead-lag controller is:

$$K(s) = G\frac{1 + sT_1}{1 + sT_2}\frac{1 + sT_3}{1 + sT_4} \tag{13}$$

In the formula, the lead link $T_1 > T_2$, the lag link $T_3 > T_4$. The specific construction method is referred to in ref. [22].

4. Simulation Verifications

Based on the PSCAD/EMTDC simulation platform, the recovery process of the centralized electric vehicle charging station participating in the black start of the power grid is simulated and verified. The detailed simulation model is shown in Figure 8. There are two centralized electric vehicle charging stations with the capacity of 0.0006 kA∗h and 0.0004 kA∗h, respectively; two generators with the capacity of 400 MVA, 100 MW auxiliary load of the power plant, and two loads of 100 MW to be started in the system.

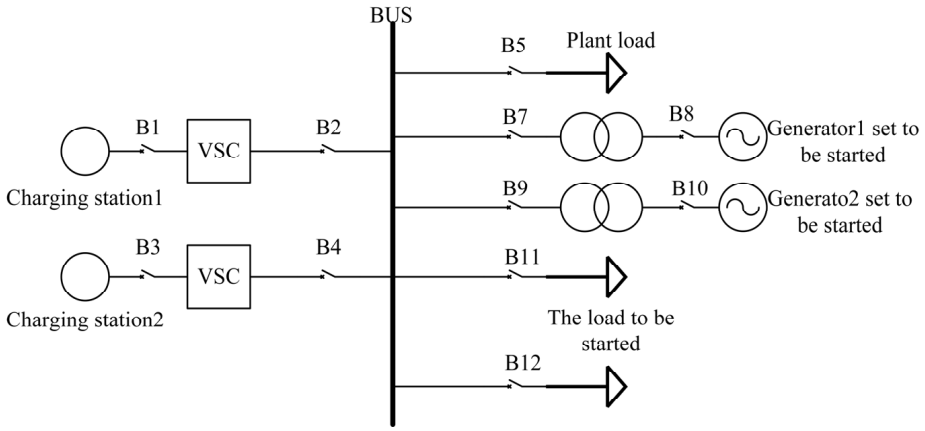

Figure 8. Simulation model for back start of Charging station combined system.

The parameters of the system are set in Table 1. To obtain the rated capacity of the charging station, we need to measure the output power of the charging station. By charging the line and starting the plant load, the active and reactive power outputs of the charging station were measured, as shown in Figure 9a,b. The energy output was calculated as shown in Figure 9c. According to Equation (5) $E_B \geq \frac{E_{0\max}-E_{0\min}}{SOC_{\max}-SOC_{\min}}$, with SOC_{max} set to 0.9 and SOC_{min} set to 0.3, considering a certain margin, the capacity of the charging station in this model, denoted as E_B, can be calculated. By converting it into parameters in PSCAD, the Rated capacity shown in Table 1 can be obtained. Based on Equation (6) $S_{vsc} \geq \max\left(\sqrt{P_B^2+Q_B^2}\right)$, the capacity of the VSC was determined. The range of initial SOC is determined based on Equation (4) $SOC_{min}+\frac{E_{0\max}}{E_B} \leq SOC_0 \leq SOC_{\max}+\frac{E_{0\min}}{E_B}$. The larger the E_B, the greater the range of initial charge allowed for the charging station's participation in grid black start. Taking into account the configuration cost of the charging station and the allowable working range, the configuration scheme shown in Table 1 was selected.

Table 1. PACAD parameters of back start of Charging station combined system.

Element	Parameters	Value
Charging station 1	Nominal voltage	400 kV
	Rated capacity	0.0006 kA∗h
	Loss of capacity at nominal current in an hour	20%
	Initial SOC	70%
Charging station 2	Nominal voltage	400 kV
	Rated capacity	0.0004 kA∗h
	Loss of capacity at nominal current in an hour	20%
	Initial SOC	90%
VSC	Rated AC voltage	230 kV
	Rated power	200 MVA
Generator1	Rated RMS Line Current	10 kA
	Rated capacity	400 MVA
Generator2	Rated RMS Line Current	10 kA
	Rated capacity	400 MVA

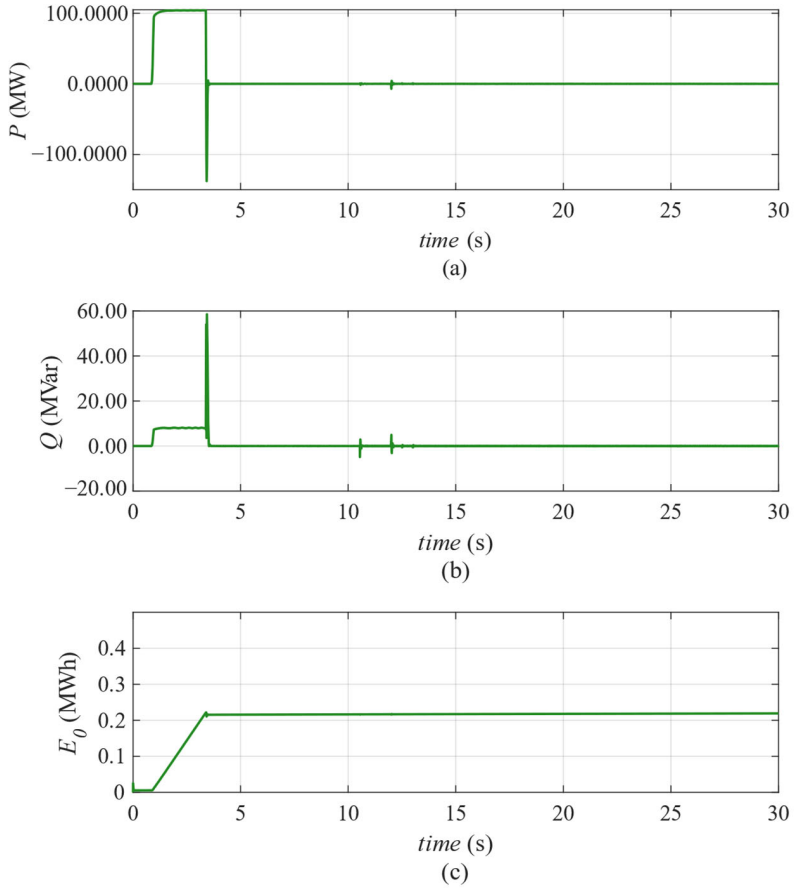

Figure 9. Active and reactive power output and the Cumulative energy output E_0 of the Charging station. (**a**) The active power output of the charging station. (**b**) The reactive power output of the charging station. (**c**) The Cumulative energy output E_0 of the Charging station.

The whole black-start process is shown in Figure 10. Firstly, Charging station1 with a larger capacity was first put into operation, and we analyzed the process of building voltage on the line with the help of the centralized electric vehicle charging station. Subsequently, Generator1 is put into operation, and the control mode of Charging station1 is switched from V/f control to P/Q additional lead-lag control during this process. Furthermore, some important loads were correspondingly put into operation before Generator2 was integrated. After the AC system SCR (Short Circuit Ratio) increased, Charging station2 was put into operation, and P/Q additional frequency control was adopted to suppress the frequency fluctuation that may have been caused by the large disturbance in the subsequent grid recovery process. In addition, a comparative simulation of the frequency fluctuation of each stage in the black start was conducted under conventional control, P/Q additional lead-lag control, and P/Q additional frequency control. Based on the comparison of the frequency fluctuation amplitude under different control modes, the advantages and disadvantages of the control modes in the black start process were compared, and the suppression effect of the additional controller on the system's low-frequency oscillation was analyzed.

4.1. Simulation Analysis of the On-Load Pressure Building Process of the Charging Station

During the early phase of the black start, the AC bus voltage and frequency were established by a centralized electric vehicle charging station. Figure 11 shows the simulated verification of the voltage and frequency changes during the establishing process, where (a) and (b) represent the simulated voltage and frequency changes, respectively. The (a) graph shows that the charging station has a good response speed when charging the line, with the VSC being put into use at 0.85 s and the line voltage can be raised to around

230 kV within 0.2 s. The (b) graph shows that the large frequency fluctuation caused by the charging station boosting process, which lasts for approximately 0.5 s, can be accepted as the system starts from a complete black state and will not affect the stability of the system. According to Figure 12, the SOC of Charging station1 drops from 70% to around 40% during this process, which means the Charging station1 transmitted power to the system in a high speed. And the requirement of black start is fast and stable, therefore, the SOC of charging station1 drops from 70% to 40% during the simulation process can be regarded as an indicator of the effective completion of the line charging task, indicating that the centralized charging station can meet the needs of the AC system for zero start-up voltage boosting with loads. This simulation process demonstrates that centralized electric vehicle charging stations can act as black start power sources and complete line charging tasks effectively.

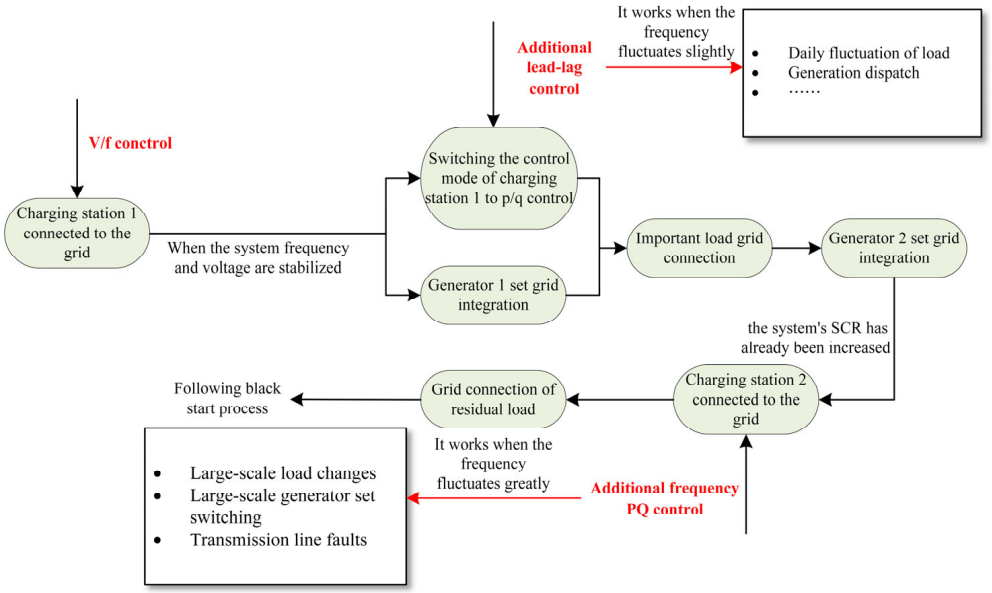

Figure 10. The black start process.

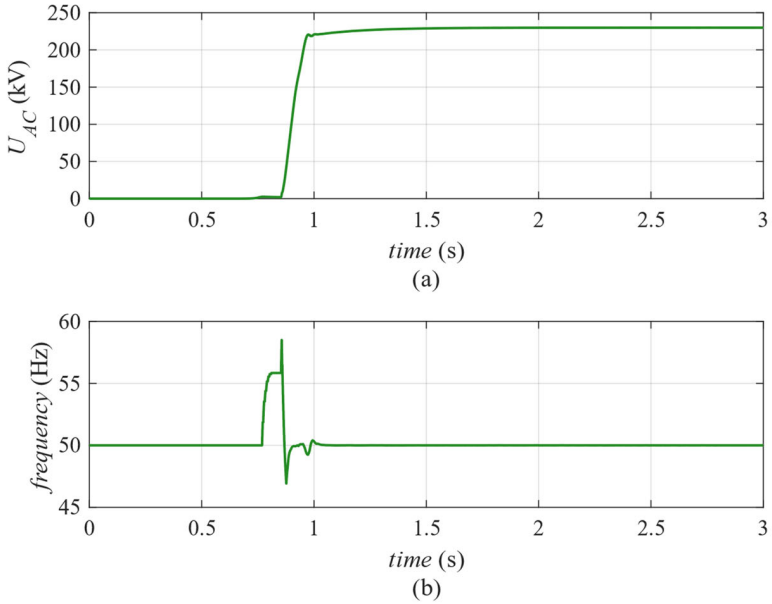

Figure 11. Line charging process. (**a**) The voltage change during the process. (**b**) The frequency change during the process.

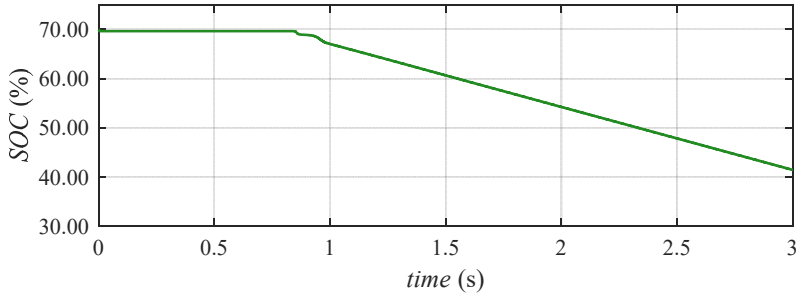

Figure 12. The change of SOC during the line charging process.

4.2. Simulation Analysis of Generator1 and Grid Connection Process

At 3.38 s, Generator1 was put into operation, and Figure 13a,b show the fluctuation changes in system voltage and frequency during its grid connection process. Figure 13a shows that the maximum fluctuation amplitude of grid voltage is 0.03 p.u. and the fluctuation size is within an acceptable range. After the oscillations, it took around 4 s to stabilize the system frequency. Since the line belongs to a lightly loaded line at this time and the capacity of Generator1 is 400 MVA, its grid connection will have a significant impact on the power system. As shown in Figure 13b, the frequency fluctuation is within 4 Hz, and 4 s later, the frequency stabilizes around 52 Hz. This fluctuation is completely acceptable during the black start process of the entire black system.

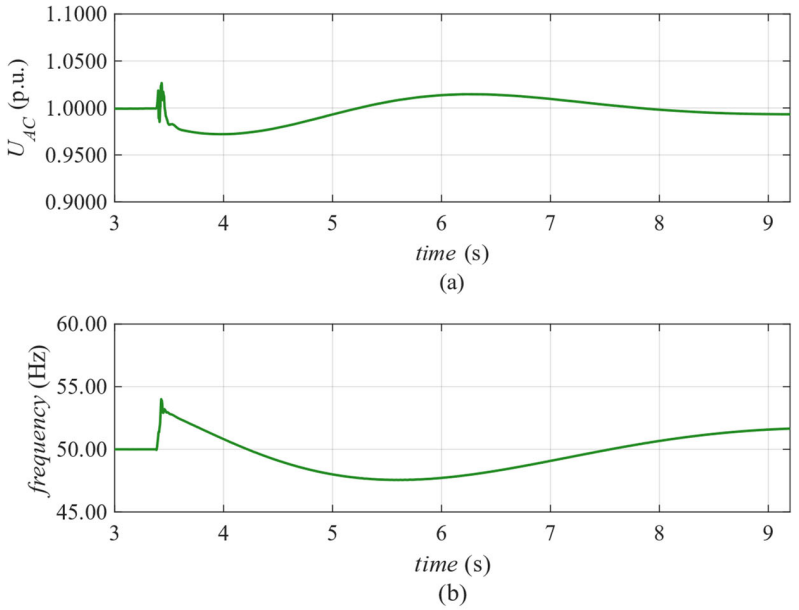

Figure 13. AC system voltage RMS change results in the process of Generator1 grid connection. (**a**) The fluctuation change in system voltage during the process. (**b**) The fluctuation change in system frequency during the process.

4.3. Simulation Analysis of Generator2 Grid Connection Process

After the system voltage and frequency were stabilized, Generator2 was connected to the grid at 10.5 s, and the fluctuation in voltage and frequency of the system was shown in Figure 14. It can be seen from (a) that the amplitude fluctuation of the system voltage during the connection of Generator2 does not exceed 0.01 p.u. In graph (b), the frequency in the figure stabilized at 52 Hz after fluctuating for about 1 s. After Generator1 and Generator2 were incorporated into the system, the total capacity of the system came to 800 MVA, and the load of the system was 100 MW, thus the load rate was 25%, which belonged to the range of light loads, so the speed of the generator rotor was too high. After the load was connected, the frequency would return to the normal level of 50 Hz.

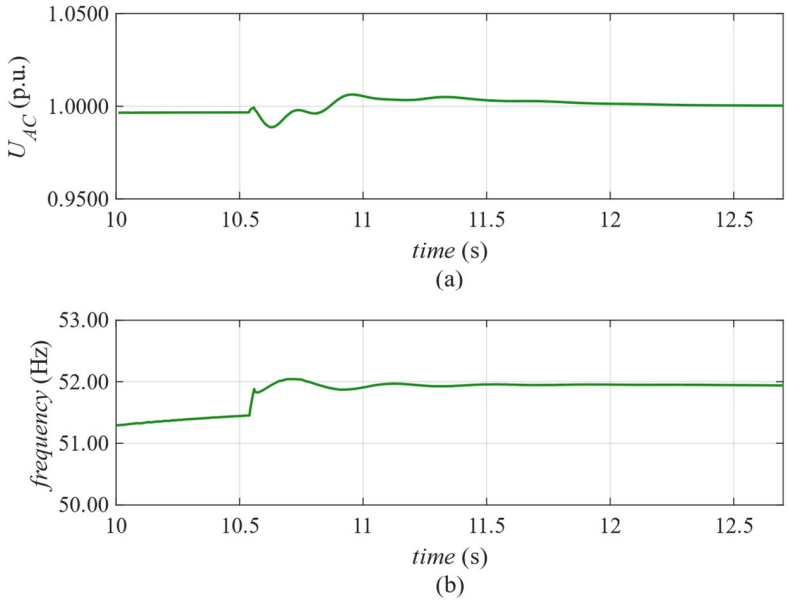

Figure 14. AC system voltage RMS change results in the process of Generator2 grid connection. (**a**) The fluctuation change in system voltage during the process. (**b**) The fluctuation change in system frequency during the process.

When comparing the grid-connected processes of Generator1 and Generator2, we can observe that Generator1 had a maximum voltage fluctuation amplitude of 0.03 p.u., while Generator2 had a fluctuation amplitude of less than 0.01 p.u. In terms of system frequency, Generator1 had a maximum fluctuation amplitude of 4 Hz, while Generator2's was less than 1 Hz. It took about 5 s for Generator1 to reach a stable state when connected to the grid, whereas Generator2 only took 1 s. The reason for this is that the system just had a rotating element of 100 MW plant load before Generator1 was connected, and the rotational inertia increased after the 400 MVA Generator1 was connected, resulting in increased stability. In general, a system with a larger rotational inertia has a better ability to withstand disturbances. Therefore, when Generator2 was connected to the grid, there was less fluctuation in voltage and frequency, and it reached stability faster. It demonstrates that the stability and regulation performance of the system improved after Generator1 was connected to the grid, allowing for an orderly black start of the power grid.

4.4. Simulation Analysis of Large Interference Suppression of Charging Station2

After the generator2 was put into operation, the system SCR increased to two times the original, enhancing the system's acceptance capacity for power injection from the DC line, thus allowing Charging Station 2 to be integrated to counteract major disturbances, such as the disconnection of high-capacity loads, and to ensure system stability during power grid restoration. When two large capacity loads were put into the grid, the comparison of the power grid frequency and voltage fluctuations that had or did not have the Charging Station 2 is shown in Figure 15. A 100 MW load was put into the system at 12.5 s, followed by another 100 MW load at 13 s.

From graph (a), we can see that the voltage oscillation amplitude of the system is reduced from 0.015 p.u. to less than 0.01 p.u. after charging station2 is put into operation at 12 s, and after 18 s, it returns to the stable value of 230 kV. Without the additional frequency control of Charging Station2, the voltage would not have reached a stable value until 25 s later. Graph (b) shows that the control of frequency fluctuation by Charging station2 was more obvious than that of voltage. When Charging Station2 was not connected, the system frequency fluctuates by more than 5 Hz and it takes until 25 s for the oscillation to end, which would greatly affect the system's stability. After Charging Station 2 was connected, the system frequency fluctuation decreased, and it ended around 17.5 s, maintaining a

frequency of 50.5 Hz, which accelerated the oscillation process of the system and was conducive to the rapid transition of the system to a new steady state. Figure 16 shows the power output of Charging Station2 during the high interference process. It can be seen that when the system is loaded with a large capacity load, the generator rotor speed cannot increase immediately to increase the active output. At this time, Charging Station2 increased the active output, adjusted the system frequency according to the frequency difference, accelerated the oscillation process, and helped the system enter a new steady state more quickly.

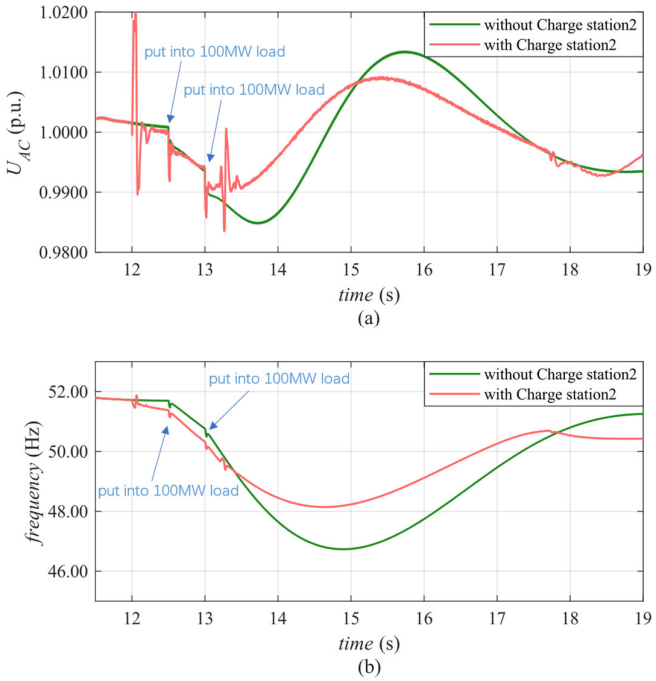

Figure 15. The effect of the additional frequency PQ control in the process of large load switching. (**a**) The effect on the system voltage. (**b**) The effect on the system frequency.

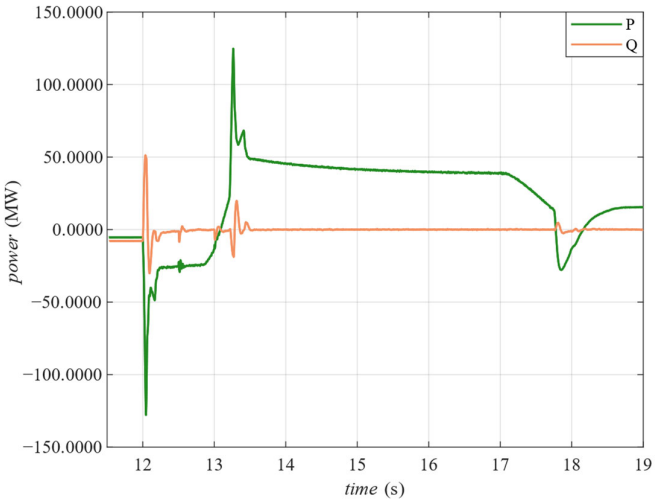

Figure 16. The power change of Charging station2 in the process of large load switching.

4.5. Simulation Analysis of Charging Station1 Control Mode Switching

After Generator1 was connected to the grid, Charging station1 immediately switched to P/Q additional lead-lag control, transferring the control of line voltage and system frequency to the generator set for control. Charging station1 itself was only used as

an auxiliary way to suppress the small disturbance of the power grid during the black start process.

The Bode diagram of the original system is shown in Figure 17, and the zero-pole diagram is shown in Figure 18. The system function is:

$$G(s) = \frac{0.004302s^4 + 3.403s^3 + 2.483s^2 - 0.09431s}{s^4 + 8.649s^3 + 6.393s^2 7.499s + 0.3531} \tag{14}$$

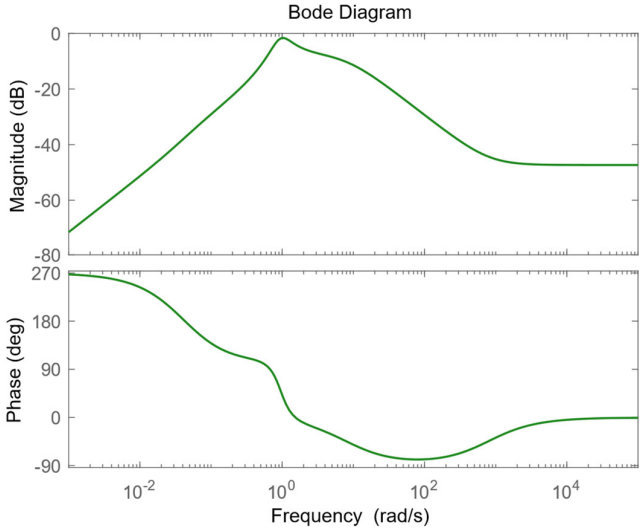

Figure 17. Bode Diagram of original system.

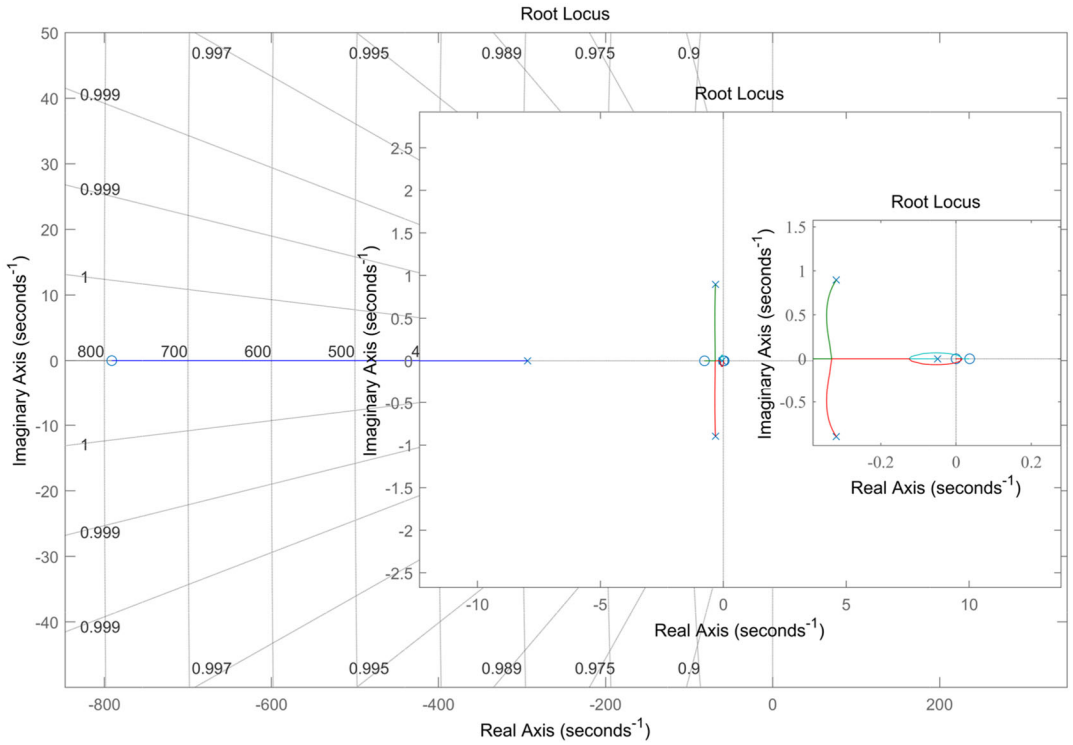

Figure 18. Pole map of original system.

According to the parameters obtained by TLS-ESPRIT identification combined with the design method in Ref. [22], the transfer function of the lead-lag controller was designed as follows:

$$G(s) = \frac{1.5s+1}{00.1s+1}\frac{0.1104s^2+0.1986s+1}{0.3625s^2+1.437s+1} \tag{15}$$

Applying the designed P/Q additional lead-lag controller to the system, the active power reference value P_{ref} of Charging station1 was increased from 1.00 p.u. to 1.05 p.u. at 7.5 s, and the effect of the controller on the system was observed. The suppression effect of the frequency deviation of the system is shown in Figure 19. In this paper, the application of the method in reference [22] is verified through simulation, and it is found that the designed additional lead-lag controller has a good suppression effect on the low-frequency oscillation that occurs during the black start process. This indicates that switching the control mode of Charging station1 from V/f to P/Q additional lead-lag control after the generator1 is connected during the black start process can improve the stability of the process.

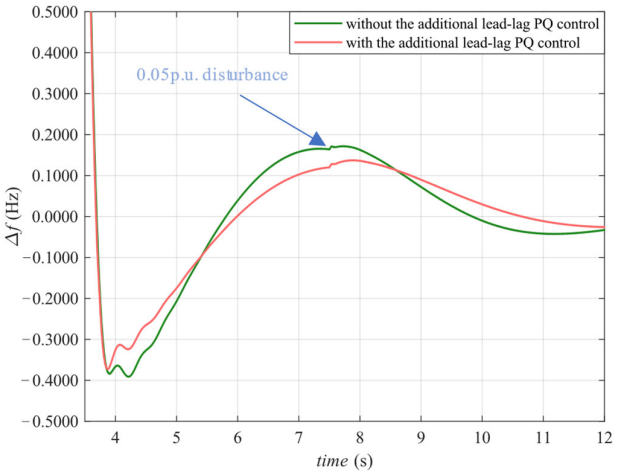

Figure 19. Frequency velocity difference diagram before and after adding controller under low frequency oscillation under small disturbance.

5. Conclusions

This article proposes a three-stage coordinated recovery strategy for black start of the power grid based on centralized electric vehicle charging stations. Based on the above analysis and simulation results, the following conclusions can be drawn.

(1) The three-stage coordinated recovery strategy of power grid black start with the participation of centralized electric vehicle charging stations proposed in this paper can effectively complete the black start of the system. The centralized electric vehicle charging station has the ability to establish the initial voltage and frequency of the AC system, which can achieve the rapid recovery of the plant load so as to start the generators and achieve smooth recovery of the power grid faster.

(2) After the grid connection of the generators, by formulating different control strategies according to the capacity of the charging station, different types of auxiliary functions of the charging station in the process of power grid restoration are realized, so that the centralized charging stations can cooperate with each other to restore the power grid more stably.

(3) The designed additional frequency control can effectively shorten the system oscillation time caused by large disturbances during the black start process; it can also accelerate its transition to a new steady state, improving the stability of the system in the black start process.

(4) The designed additional lead-lag controller has a good suppression effect on the low frequency oscillation during the black start process, maintaining the voltage and frequency within a stable range and improving the reliability and safety of the black start process.

To a certain extent, the black start coordinated recovery strategy verified in this paper expands the exploration of the demand response between the centralized electric vehicle charging station and the power grid. In the future trend, the wide application of electric vehicles will increase the number of centralized electric vehicle charging stations. When multiple charging stations cooperate with each other, there will be more control strategy combinations, and the reliability of charging stations as black start power supplies will be greatly improved.

Remarkably, the system built in this paper is still relatively simple, far less complex than the actual power grid, so this paper only provides a new choice of black start power supply and studies its coordinated control strategy, which can be used as a reference to realize the rapid and stable recovery of the power grid. Future research directions can focus on more coordinated control strategies for charging stations, such as robust control, droop control, etc. Or taking a single electric vehicle as the main part to participate in the black start of the power grid is also a feasible direction, which can better explore various application scenarios of electric vehicles and related equipment in the power system.

Author Contributions: Conceptualization, M.W. and B.L.; methodology, M.W. and B.L.; software, M.W. and B.L.; validation, M.W. and B.L.; data curation, M.W. and B.L.; writing—original draft preparation, M.W.; writing—review and editing, M.W., C.D. and B.L.; supervision, B.L.; project administration, T.L., B.L. and Q.J.; funding acquisition, H.S. All authors have read and agreed to the published version of the manuscript.

Funding: This work is supported partially by the Opening Fund of Power Internet of Things Key Laboratory of Sichuan Province (The Novel Adaptive Recovery Technology for Power Systems Based on Dynamic Measurement, PIT-F-202310), partially by the Special Fund for Basic Scientific Research Business Expenses of Central Universities (2022SCU12005) and is also supported by the General Project of Natural Science Foundation of Sichuan Province (2022NSFSC0262).

Data Availability Statement: Not applicable.

Conflicts of Interest: The authors declare no conflict of interest.

References

1. Adibi, M.; Clelland, P.; Fink, L.; Happ, H.; Kafka, R.; Raine, J.; Scheurer, D.; Trefny, F. Power System Restoration—A Task Force Report. *IEEE Trans. Power Syst.* **1987**, *2*, 271–277. [CrossRef]
2. Zhang, C.; Wei, Y.L.; Cao, P.F.; Lin, M.C. Energy Storage System: Current Studies on Batteries and Power Condition System. *Renew. Sustain. Energy Rev.* **2018**, *82*, 3091–3106. [CrossRef]
3. Yilmaz, M.; Krein, P.T. Review of the Impact of Vehicle-to-Grid Technologies on Distribution Systems and Utility Interfaces. *IEEE Trans. Power Electron.* **2013**, *28*, 5673–5689. [CrossRef]
4. Liu, H.; Qi, J.; Wang, J.; Li, P.; Li, C.; Wei, H. EV Dispatch Control for Supplementary Frequency Regulation Considering the Expectation of EV Owners. *IEEE Trans. Smart Grid.* **2018**, *9*, 3763–3772. [CrossRef]
5. Li, Y.; Ren, X.; Ni, Z.; Zhao, T.; Ge, L.; Li, X.; Luo, Y.; Zhao, Y. Shared Energy and Reserve Based Coordinated Operation Between Electric Vehicle Charging Stations and Distribution Power Network. *IEEE Trans. Ind. Appl.* **2023**, 1–13. [CrossRef]
6. Corinaldesi, C.; Lettner, G.; Schwabeneder, D.; Ajanovic, A.; Auer, H. Impact of Different Charging Strategies for Electric Vehicles in an Austrian Office Site. *Energies* **2020**, *13*, 5858. [CrossRef]
7. Zhang, C.; Meng, J.; Cao, Y.; Huang, Q.; Jing, S.; Liu, Q. A Battery Swapping Requirement Adequacy Model for Electric Vehicles and Its Simulation Research. *Power Syst. Technol.* **2012**, *36*, 15–19.
8. Liu, Y.; Fan, R.; Terzija, V. Power System Restoration: A Literature Review from 2006 to 2016. *J. Mod. Power Syst. Clean Energy* **2016**, *4*, 332–341. [CrossRef]
9. Gu, X.; Li, X.; Yang, C.; Li, S. Black Start Scheme Considering Wind Power Participation. *Electr. Power Autom. Equip.* **2020**, *40*, 31–37. [CrossRef]
10. Tongge, L.; Yonghong, H.; Junyi, M.; Yimin, X. The Research on Black Start Strategy of Distributed Photovoltaic-Battery Energy Storage Systems Based on Cluster Division. In Proceedings of the iSPEC 2020—IEEE Sustainable Power and Energy Conference: Energy Transition and Energy Internet, Chengdu, China, 23–25 November 2020.
11. Li, J.; Xiao, Q.; He, G.; Fu, Y. Distribution Network Island Partition and Black Start Based on Distributed Generation. *J. Phys. Conf. Ser.* **2021**, *1871*, 012044. [CrossRef]
12. Zhang, Y.; Wu, J.; Jiang, Q.; Li, B.; Gou, H.; Wang, T.; Zhang, M. Receiving-End Power Grid Black Start Technology and Coordinated Restoration Strategy Based on Wind-Storage Combined System. *Adv. Eng. Sci.* **2023**, *55*, 72–83. [CrossRef]

13. Sun, L.; Wang, X.; Liu, W.; Lin, Z.; Wen, F.; Peng Ang, S.; Salam, M.A. Optimisation Model for Power System Restoration with Support from Electric Vehicles Employing Battery Swapping. *IET Gener. Transm. Distrib.* **2016**, *10*, 771–779. [CrossRef]
14. Tremblay, O.; Dessaint, L.A.; Dekkiche, A.I. A Generic Battery Model for the Dynamic Simulation of Hybrid Electric Vehicles. In Proceedings of the VPPC 2007—IEEE Vehicle Power and Propulsion Conference, Arlington, TX, USA, 9–12 September 2007; pp. 284–289. [CrossRef]
15. Wang, Y.; Qiu, F.; Liu, G.; Lei, M.; Yang, C.; Wang, C. Adaptive Reference Power Based Voltage Droop Control for VSC-MTDC Systems. *J. Mod. Power Syst. Clean Energy* **2023**, *11*, 381–388. [CrossRef]
16. Bao, P.; Zhang, W.; Zhang, Y. Secondary Frequency Control Considering Optimized Power Support From Virtual Power Plant Containing Aluminum Smelter Loads Through VSC-HVDC Link. *J. Mod. Power Syst. Clean Energy* **2023**, *11*, 355–367. [CrossRef]
17. Liu, L. Research on the Control Technology of Energy Storage Wind Farms as a Black Start Power Source for the Grid. Ph.D. Thesis, North China Electric Power University, Beijing, China, 2017.
18. Liu, Q.; Shi, L.-B.; Ni, Y.-X.; Dong, Z.-Y. Intelligent Optimization Strategy of the Power Grid Reconfiguration During Power System Restoration. *Proc. CSEE* **2009**, *29*, 8–15. [CrossRef]
19. Shang, L.; Dong, X.; Liu, C.; Gong, Z. Fast Grid Frequency and Voltage Control of Battery Energy Storage System Based on the Amplitude-Phase-Locked-Loop. *IEEE Trans. Smart Grid* **2022**, *13*, 941–953. [CrossRef]
20. Lei, T.; Lü, F.; Liu, J.; Zhang, L.; Zhou, T.; Bao, X. Inertia and Damping Characteristics of DFIG and Improved Additional Frequency Control Strategy. *Electr. Power Autom. Equip.* **2022**, *42*, 190–196. [CrossRef]
21. Samal, S.K.; Subudhi, B. New Signal Subspace Approach to Estimate the Inter-Area Oscillatory Modes in Power System Using TLS-ESPRIT Algorithm. *IET Gener. Transm. Distrib.* **2019**, *13*, 4123–4140. [CrossRef]
22. Datta, U.; Kalam, A.; Shi, J. Battery Energy Storage System to Stabilize Transient Voltage and Frequency and Enhance Power Export Capability. *IEEE Trans. Power Syst.* **2019**, *34*, 1845–1857. [CrossRef]